MECCA

Journal of Middle European Construction and Design of Cars

Number 01 2017, volume XV.

165 Kč / 11€

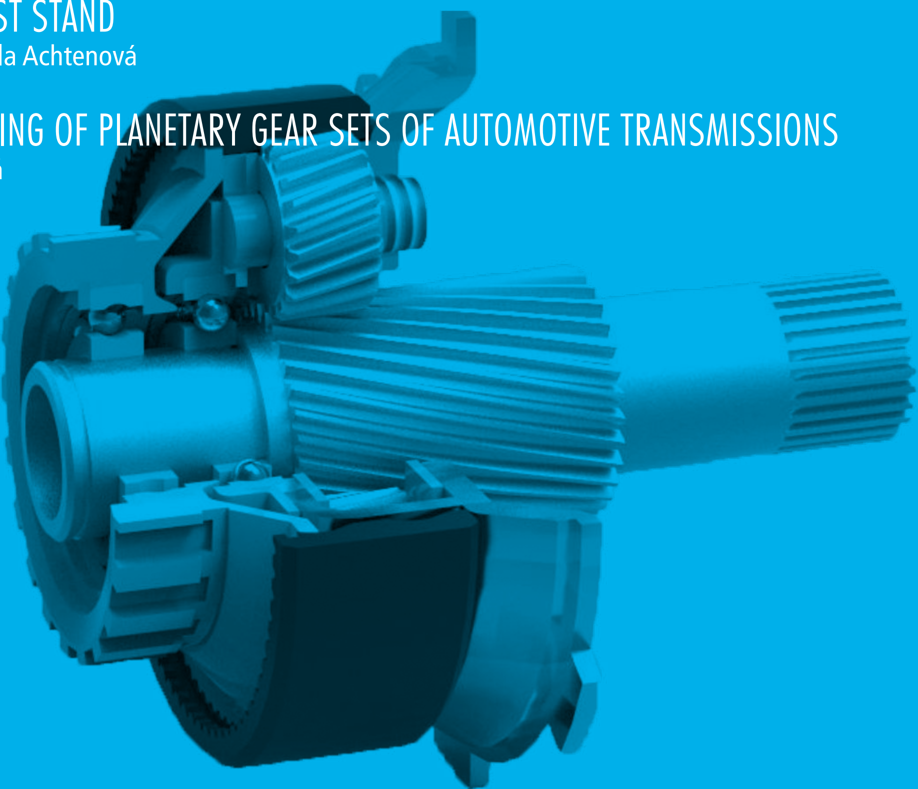

9 771214 082007

THIS ISSUE IS FOCUSED ON RESEARCH IN: DESIGN OF VEHICLES

AIM
Published in the heart of Europe on Czech Technical University in Prague the journal reports about research in the field of internal combustion engines and all other components and aspects of vehicle engineering and vehicle design. The articles from the whole world are welcome.

THE FOLLOWING TOPICS ARE RELEVANT FOR THE JOURNAL MECCA:
- Engines and fuels
- Powertrains (hybrid vehicles, transmissions,...)
- Chassis
- Vehicle body
- Experimental testing
- Mechatronics
- Vehicle dynamics
- Safety
- Transport Systems
- Electronics in vehicles

PERIODICITY
Three times a year

REVIEW PROCESS
All articles are peer and blind reviewed. At least two reviewers per article.

LANGUAGE
English, bilingual abstract and legends (English/Czech or English/Slovak). Articles coming from non-English speaking coutries are submitted to English correction.

ABSTRACTING AND INDEXING
The journal is part of database of open access publications (DOAJ): https://doaj.org/toc/1804-9338
Publisher of the open access articles: De Gruyter.

This journal is published using financial support from the budget of the Centre of Vehicles for Sustainable Mobility, Faculty of Mechanical Engineering, Czech Technical University in Prague. A part of support comes from the project Josef Božek Competence Centre for Automotive Industry TE 0102 0020, funded by the Technological Agency of Czech Republic. These sources are gratefully acknowledged.

Josef Božek Competence Centre for Automotive Industry

Technology Agency of the Czech Republic

Centers of Competence

IMPRINT MECCA – VOLUME XV, NUMBER 01, YEAR 2017, http://bozek.cvut.cz/mecca, gabriela.achtenova@fs.cvut.cz
Editor: České vysoké učení technické v Praze MECCA, Technická 4, 16607, Praha 6, Czech republic, **ISSN 1214-0821, ISSN 1804-9338 (Online), MK ČR E 13720**
Proofreading: Channel Crossings, Prague, Czech Republic **Advertising:** gabriela.achtenova@fs.cvut.cz or jan.macek@fs.cvut.cz **Production/Layout:** studio pixl-e (studio@pixl-e.cz)

DE GRUYTER OPEN

10.1515/mecdc-2017-0001

COMPOSITE ABSORBER IN COLLISION SIMULATIONS OF A BUS

VÍT SHÁNĚL
Faculty of Mechanical Engineering, Czech Technical University in Prague, Technická 4, Prague, +420 224 35 2519, vit.shanel@fs.cvut.cz

MIROSLAV ŠPANIEL
Faculty of Mechanical Engineering, Czech Technical University in Prague, Technická 4, Prague, +420 224 35 2561, miroslav.spaniel@fs.cvut.cz

ABSTRACT
This paper details the numerical modeling of composite absorbers and an assessment of the influence of such deformation elements on a bus during frontal collision with a car. The absorber itself is designed as an assembly of thin-walled composite wound tubes oriented in the vehicle direction of travel. During the impact the tubes are crushed, causing energy absorption. Crash simulations were performed at various speeds using differing scenarios with the deformational member as well as without it. Comparative diagrams of force and velocity of the car and deformation of the bus structure were assessed.
KEYWORDS: ABSORBER, CRASH, FEM, SIMULATION

SHRNUTÍ
Článek se zabývá vývojem numerického modelu kompozitního absorbéru a posouzením vlivu celého deformačního členu autobusu při jeho čelním nárazu s osobním automobilem. Absorbér je navržen jako soubor tenkostěnných vinutých kompozitových trubek orientovaných ve směru jízdy. V momentě nárazu nastane borcení těchto trubek a tím dojde k významné absorpci energie. Byly provedeny simulace nárazu při různých rychlostech ve variantách při použití deformačního členu a bez něj. Porovnáním průběhů sil, rychlostí a posuvů osobního automobilu a deformací konstrukce autobusu byla posouzena jeho funkce.
KLÍČOVÁ SLOVA: ABSORBÉR, NÁRAZ, MKP, SIMULACE

1. INTRODUCTION
Mass reduction is one of the frequently-mentioned requirements for both current and future vehicles. Substitution of various previously steel or alloy parts with composite ones is a commonly accepted approach to this problem. This article presents a numerical study of a specific kind of impact energy absorber made from composite parts. It is based on the experimentally determined response of a single energy absorbing component. The response of the complete absorber, or the vehicle-absorber assembly, has been determined numerically.

The purpose of this task was to verify the use of a thin bundle of wound composite tubes to absorb impact energy. The initial task was a series of experimental impact tests on individual tubes and small bunches of tubes in order to determine their response [3]. We have tested several layup options to find the layup that is characterized by stable crushing, a small peak force at the beginning, and a high energy absorption rate. Subsequently, we formulated a computational model at the level of the tube with a more complex material model including a description of the damage to the composite [2]. Using the Abaqus software, we were unable to create a tube model with responses consistent with the experiments. However, such a complicated model at the tube model level would not be applicable to any collision simulation with vehicles containing the absorber (which would consist of a significant number of these composite tubes). For this reason, a simplified tube model as described below was created. This model describes the crushing of the composite tube in a way that is sufficiently accurate and corresponds with the experimentally observed behavior. This tube model is adapted to simulate vehicle collisions containing several tens of composite tubes.

FIGURE 1: Crash simulation arrangement.
OBRÁZEK 1: Uspořádání simulace nárazu.

The objective of the car-bus frontal impact simulation is to assess the impact absorber (i.e. deformational member) composed of composite tubes that serve as deformation elements of the respective member and absorb the kinetic energy. The simulation of this impact is highly complex and thus certain simplifications of the problem are vital. Nevertheless, the situation still provides a solid functional rendition of the absorber during a frontal collision between a bus and a car. The crash simulation arrangement is shown in Figure 1, where 1 is the car, 2 is the absorber, and 3 is the bus. The simulation was performed using ABAQUS/Explicit.

2. CRASH SITUATION

The crash simulation is performed using three models of interacting bodies: the model of the bus, the model of the vehicle, and the model of the absorber. Each model includes a certain degree of simplification compared to reality. The main simplification is an absolutely rigid car model with boundary conditions that prevent it from sliding and turning in other directions than its displacement perpendicular to the bus front. Similarly, the properties and the deformation of the absorbers are enabled only in this direction – in Figure 1 depicted as the x-direction. Only the front half of the bus is used in the simulation. The car has an initial velocity and the bus was fixed at the end of its front half.

For this impact simulation, a simplified model of a car was created – Figure 1. The car is represented by an absolutely rigid block which is 1188 mm wide, 500 mm high and shaped just like the car bumper. This block is assigned a weight of 1444 kg. The front half of the standard bus model used for crash simulation in the PAM-Crash software was used. This model is based on shell elements with elastic-plastic behavior.

3. MODEL OF THE DEFORMATION ELEMENT

Deformation elements in the absorber are wound composite tubes which are located at the front of the bus. The tubes are made of carbon fiber and an epoxy matrix. Mechanical properties (force-displacement diagram) of this composite tube during crushing were obtained from dynamic experiments on a drop tester. A simplification of the recorded behavior is shown in Figure 2. The force-displacement behavior shows an apparent initial peak with the maximum force of 25 kN and the force response has a steady value of 20 kN during stable crushing.

The behavior of this deformation element can be introduced into the FEM model in ABAQUS using the connector element (Connector type Translator). Using this feature, a force-displacement response can be prescribed – but only in a limited way. In order to obtain identical force-displacement response, it is necessary to use two connector elements with different behaviors and join them together. Then we can

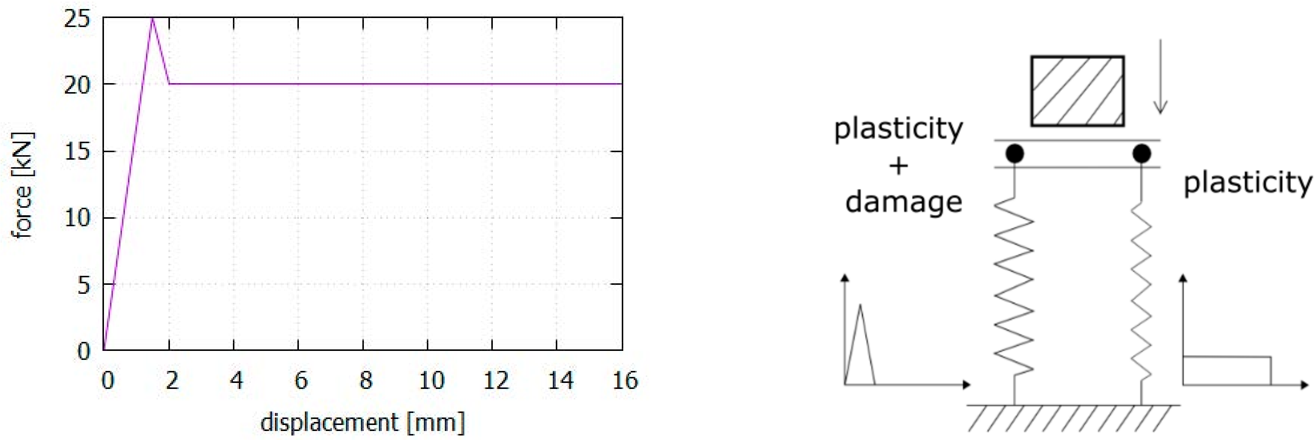

FIGURE 2: Diagram of the deformation element model and its force-displacement response.
OBRÁZEK 2: Schéma modelu a odezva deformačního elementu.

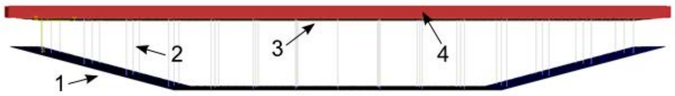

FIGURE 3: Absorber and its parts (top view).
OBRÁZEK 3: Absorber a jeho části (pohled seshora).

achieve the same deformation element behavior as obtained from the experiments.
The first connector element describes the initial peak of the force-deformation behavior, and the second connector displays stable crushing. Parallel connection of both connectors (Figure 2) ensures a model with the same force-displacement behavior as we obtained on a drop tester.
The connector element describing the first peak has the following properties. The elastic response is deactivated and all behavior derives from plasticity with some damage. The plasticity limit (yield) is set to 5 kN and initiation of damage is also set at 5 kN. A second connector element simulating stable crushing is also without elastic response and exhibits only plastic behavior, which is set to 20 kN.

4. MODEL OF THE ABSORBER

Deformation elements described above are inserted into the deformational member – the absorber (Figure 3), which is placed at the front of the bus. The absorber consists of four parts: 1 – front plate, 2 – deformation elements, 3 – rear plate, 4 – supporting structure.
The front and back plates do not have a significant impact on absorber behavior – their function is to keep the deformation elements in place and cover them. The supporting structure at the back of the absorber is an intermediate stage between the deformation elements and the bus frame. Its function is to ensure uniform transfer of the forces occurring during crushing of the deformation elements into the structure of the bus.
The absorber used in the simulations has a width of 2280 mm, a height of 480 mm and a depth between 100 mm and 250 mm. The whole absorber is divided into three parts, two outer and one central part. The central part occupies half the width of the absorber and has a constant depth of 250 mm. The depth of the outer arrays of half the size of the central part varies linearly from 250 mm inside to 100 mm at the edge of the absorber. The absorber is composed of 45 deformable elements described above, which are uniformly distributed over its area.
The proposed absorber is theoretically able to absorb an energy of approximately 200 kJ, assuming maximum deformation of the deformation elements. This absorber is placed at the frontal bottom part of the bus where it absorbs a significant part of the energy resulting from a frontal impact with a car.

5. RESULTS

Six simulations of impact with different conditions were performed: using different initial car speeds, using the absorber, or omitting the absorber. We monitored the progress of displacement, velocity and acceleration of the car. The monitored variables on the bus were logarithmic deformation and reaction forces in the restrained half of the bus.
Progress of the car velocity after impact for all variants is shown in Figure 9. For all variants velocity reduction is more significant in cases using the absorber. Therefore, the impacting bodies achieve zero velocity earlier at all initial speeds than in situations where the absorber is not used. The second graph, Figure 9, shows the progress of the reactionary forces in the half of the bus where the boundary condition is applied – these forces are transmitted in the half of the bus frame.
The following four images show the distribution of the largest main logarithmic strain in the front of the bus from the bottom view after the impact. All images have the same range of deformations – from zero to two percent of the logarithmic deformation. The displayed situation is captured at the end of the impact – the car is no longer in contact with the bus. Grey areas represent a logarithmic deformation greater than two percent.
At higher initial velocities (30 and 40 km/h), buckling of the front structure of the bus is clear. The rigidity of this part is not sufficient and thus fails before transmitting the necessary force to support the absorber during its function. This is shown in Figure 7 with the logarithmic strain for an impact with initial velocity of 40 km/h.
In the case of the 20 km/h initial speed, we could see the loading design nodes responsible for transmitting forces generated by the absorber to the rest of the structure. At this initial speed there was no significant damage, and it was therefore omitted from the list.
Based on the results, it is evident that the front part of the bus is currently designed as a deformation zone and not as a rigid part of the structure intended to transfer and distribute forces arising from an impact to the rest of the structure.
When comparing impact results with and without the absorber, the difference in energy absorption becomes very obvious. When the absorber is not installed on the bus structure (Figures 4 and 6) all of the impact energy must be absorbed by the plastic deformation of the bus frame. There is significant deformation and lower rigidity of the front part of the structure as well as a notable bending of the bus structure causing a longer energy absorption time.

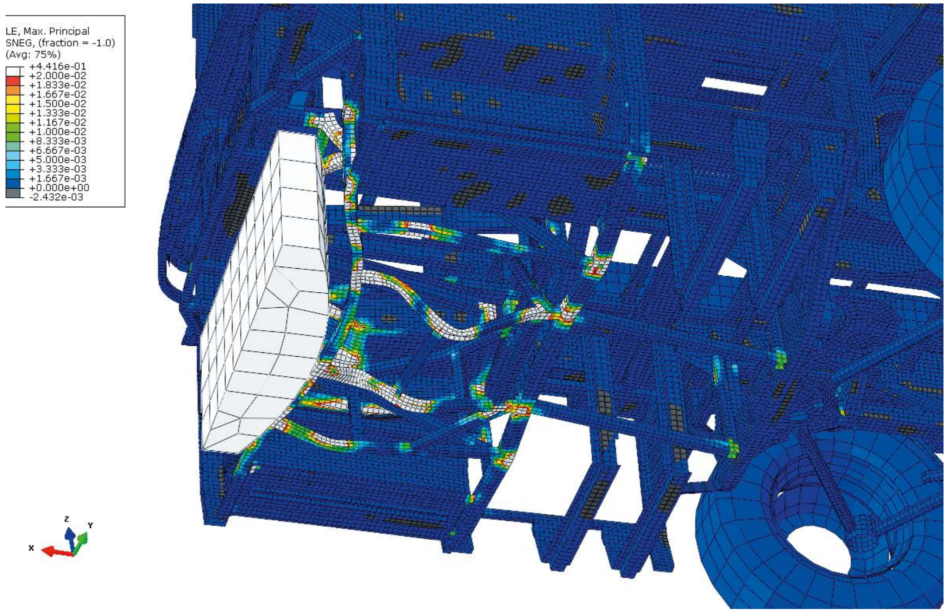

FIGURE 4: Logarithmic strain of the bus after car impact with initial velocity 30 km/h without the absorber.
OBRÁZEK 4: Logaritmická deformace konstrukce autobusu po nárazu autem rychlostí 30 km/h bez absorbéru.

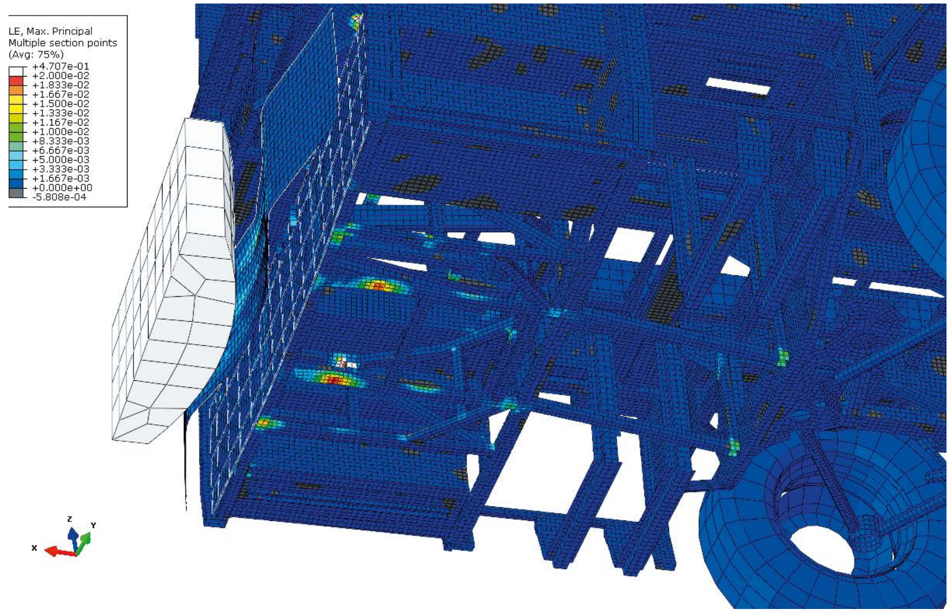

FIGURE 5: Logarithmic strain of the bus after car impact with initial velocity 30 km/h with the absorber.
OBRÁZEK 5: Logaritmická deformace konstrukce autobusu po nárazu autem rychlostí 30 km/h s absorbérem.

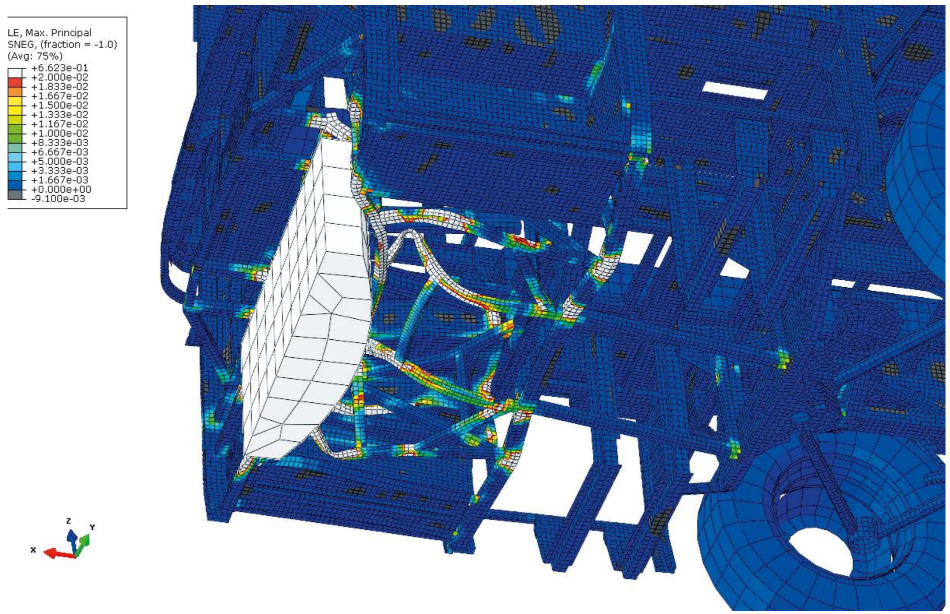

FIGURE 6: Logarithmic strain of the bus after car impact with initial velocity 40 km/h without the absorber.
OBRÁZEK 6: Logaritmická deformace konstrukce autobusu po nárazu autem rychlostí 40 km/h bez absorbéru.

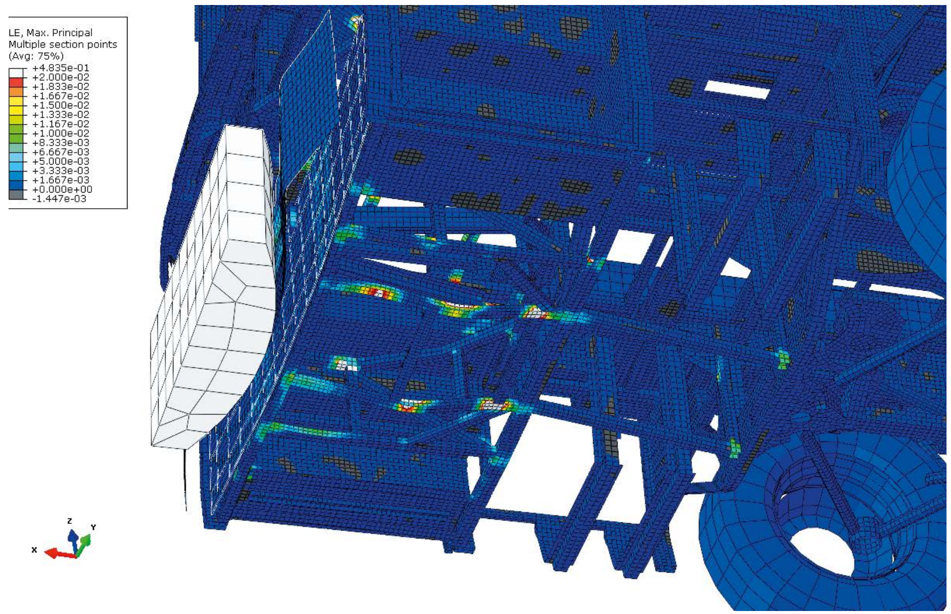

FIGURE 7: Logarithmic strain of the bus after car impact with initial velocity 40 km/h with the absorber.
OBRÁZEK 7: Logaritmická deformace konstrukce autobusu po nárazu autem rychlostí 40 km/h s absorbérem.

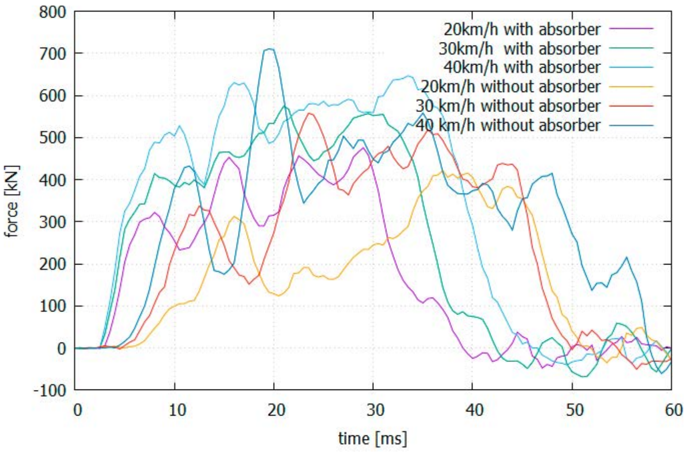

FIGURE 8: Reaction force in the half of the bus over time.
OBRÁZEK 8: Graf závislosti reakční síly ve vetknutí autobusu na čase.

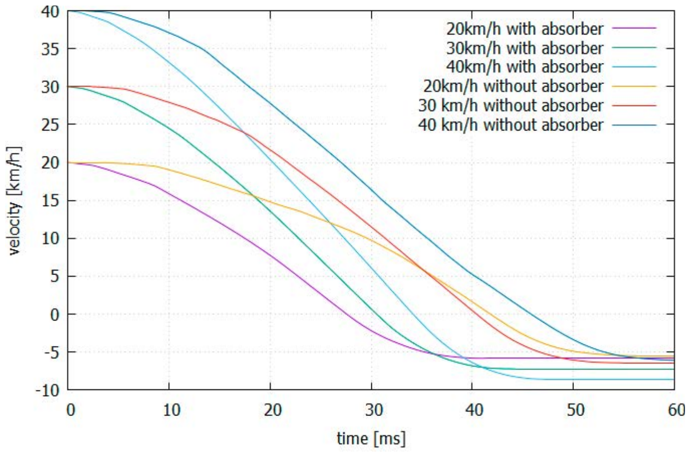

FIGURE 9: Graph of the car velocity over time for all variants.
OBRÁZEK 9: Graf závislosti rychlosti automobilu na čase pro všechny varianty.

6. CONCLUSION

Six simulations of a head-on collision between the bus and a car were performed, outlining a possible course of development of the given situation. The aim of the simulations was to assess the impact absorber installation on the front of the bus. This assessment was made by comparing the deformation and forces of the bus and velocity of the car. The simulations do not aim to cover every possible situation that might arise from the collision of a car and a bus. The special case of a direct collision using a simplified model of a car was selected in order to test the absorber effect during the collision. There is a clear positive role of the absorber as a deformation member. However, at higher velocities the rigidity of the front structure of the bus is insufficient. It is necessary to reinforce the front part of the bus structure for the real usage of the absorber on a bus.

ACKNOWLEDGEMENTS

This study was supported by the grant project Josef Božek Centre of Competence of Automotive Industry (2012 – 2017), TE01020020.

REFERENCES

[1] Abaqus 6.14 Documentation.

[2] Bogomolov S., Kulíšek V., Španiel M., Růžička M. (2011) FE Simulation of Composite Structure, In: Calculation of structures using FEM, Plzeň, pp. 25-32. ISBN: 978-80-261-0059-1.

[3] Sháněl V., Kulíšek V., Růžička M. (2013) Experimental Testing of the Composite Energy Absorber, In: Advanced Materials Research, Vol. 717, pp 320-324

DE GRUYTER OPEN

10.1515/mecdc-2017-0002

DYNAMIC TESTING OF BUSES AND THEIR COMPONENTS

PETR ZÁRUBA
TÜV SÜD Czech, Novodvorska 994/138, 142 21, Prague, Czech republic, +420 607 068 202, petr.zaruba@tuv-sud.cz

JAKUB JELÍNEK, MICHAL KALINSKÝ
TÜV SÜD Czech, Novodvorska 994/138, 142 21, Prague, Czech republic, jakub.jelinek@tuv-sud.cz, michal.kalinsky@tuv-sud.cz

ABSTRACT
The article gives an overview of a virtual simulation method under ECE Regulation No. R66 – bus rollover. The first part of the article introduces the process of virtual simulations in terms of homologation. The conclusion is focused on the correlation of physical tests with virtual simulations.
KEYWORDS: ECE NO. 66, ROLLOVER TEST, FEM ANALYSIS, CRASH, PHYSICAL TESTING, VALIDATION, AUTOMOTIVE, TÜV SÜD CZECH

SHRNUTÍ
Článek se věnuje problematice virtuálních simulací dle předpisu ECE No. R66 – převrácení autobusů. V jednotlivých kapitolách je rozebrán postup virtuálních simulací z pohledu metodiky a homologačního procesu. Závěr je věnován korelaci fyzických testů s virtuálními simulacemi.
KLÍČOVÁ SLOVA: EHK 66, PEVNOST KAROSERIE, PŘEVRÁCENÍ AUTOBUSU, MKP ANALÝZA, DYNAMICKÉ DĚJE, FYZICKÉ TESTOVÁNÍ, VALIDACE, AUTOMOTIVE, TÜV SÜD CZECH

1. INTRODUCTION

Every year sees an increase in the requirements for passive vehicle safety, and not just in the personal vehicles category, but also for public transport vehicles. TÜV SÜD Czech has been certifying M2 and M3 category buses (single deck rigid or articulated vehicles) according to European regulation ECE R66 – Strength of the chassis large bus, for several years. Regulation ECE R66 is one of several homologation regulations which can be certified by virtual simulation. Virtual simulations are very much required with this regulation, because physical tests take a long time to perform and do not allow many iterations of conceptual design within a very short timeframe.

2. REGULATION ECE R66

Regulation ECE R66 entered into force in 1989. In 2005, a series of changes included more detailed approval procedures using virtual simulations. Regulation R66 requires a manufacturer to construct the chassis of vehicles that will carry more than 22 passengers including driver strong enough so that a survival space clear of any penetration by internal primary structure is preserved when it falls from a platform. This survival space for passengers and driver is defined by the floor structure, the inner cover of the main load structure and by definition of the SR point on the seat, see Figure 2. The test is performed with only half the mass of all passengers, which is 34 kg per passenger, located 100mm before and above the R point of the seat. This stricter regulation with added mass is described in R66.01 only for newly certified vehicles with effect from November 2010. In November 2017, however, a new version of regulation R66.02 was introduced that extends compliance with this regulation to smaller buses (16+ passengers).

3. CERTIFICATION PROCESS USING VIRTUAL SIMULATION

The process of certification by virtual simulation requires the time consuming and sophisticated preparation of a numerical model. This method depends on having the full set of data

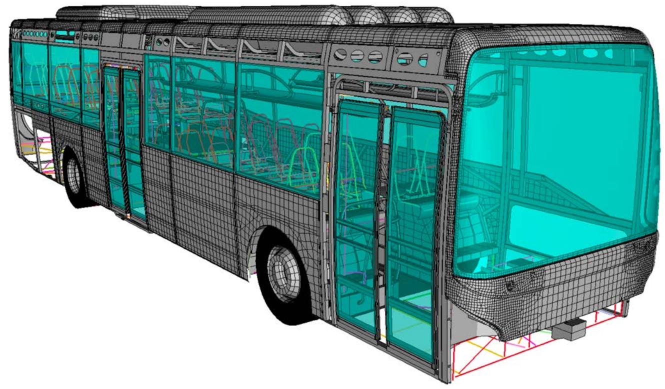

FIGURE 1: FEM model of bus
OBRÁZEK 1: MKP model autobusu

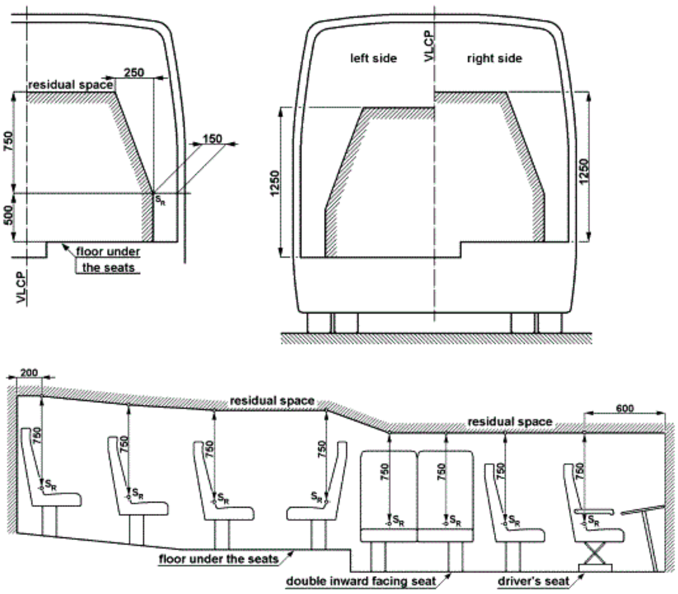

FIGURE 2: Survival space template
OBRÁZEK 2: Vymezení prostoru pro přežití

from manufacturer, such as 3D CAD data, real mass of bus components, exact position of the center of gravity, and material characteristics. From the certification point of view the manufacturer may place on the market several variants of the same vehicle type for different numbers of passengers. For this type of global approval, the worst-case configuration for the rollover strength test is considered for the calculation as it covers all other less severe designs. This is the construction with theoretically the worst deformation. The basic structural elements of bus construction are steel beams on the side of the bus and it is, in particular, the number of these beams that determines the stiffness of bus during rollover. From experience the worst variants are those that have a lower number of side beams and the highest center of gravity. When the CoG point is high on the Z axis, the impact energy and angular speed is also increased and causes bigger deformations. To determine the worst variants, a method based on the calculation of the impact energy and its relationship to specific columns with the inclusion of the cross-sectional characteristic is used. The variant with the highest energy at the column is deemed the worst case.

With the updated version of the regulation, the standard now also applies to buses with low transport capacity. These vehicles are conceptually very different because they use self-supporting or additionally reinforced van structures, see Figure 3. For these vehicle types it is very difficult to use the simple principle of relative strain energy on a pillar adopted for conventional buses. The choice of the most critical variant is determined primarily by the position of the center of gravity, the transport capacity and the equipment of the bus – its operating mass.

The chassis of these bus types (vans) do not perform at their best during the R66 test. The main objective of bus manufacturers is to maximize transporting capacity and, with a typical number of 30 passengers, the vehicle mass of a tested vehicle is increased by more than one ton of additional mass. This is in some cases almost a quarter of the mass of the structure, which is located above the original center of gravity. Compared to large buses, it is much more difficult to feasibly design this type of vehicle from the manufacturer's perspective given the complication of adding additional beams into the existing structure.

The manufacturer is required to submit the necessary documentation for this vehicle variant. Then the certification process takes place according to the internal methodology. If a manufacturer cannot provide the testing laboratory with approved material data sheets, the window beams have to be physically tested and a material model developed. Several tests have to be carried out and these are quasi-static tensile tests, bending tests and dynamic drop tests. Dynamic drop tests are primarily performed to determine the response of a material during impact. The mechanical properties of the material vary with the load speed (the strain-rate effect). This

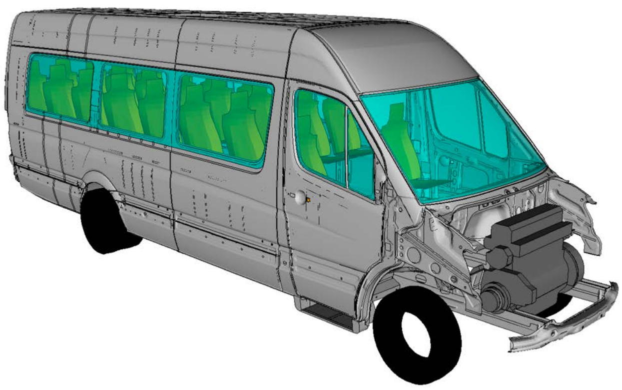

FIGURE 3: Van type of vehicle
OBRÁZEK 3: Autobus založený na podvozku dodávky

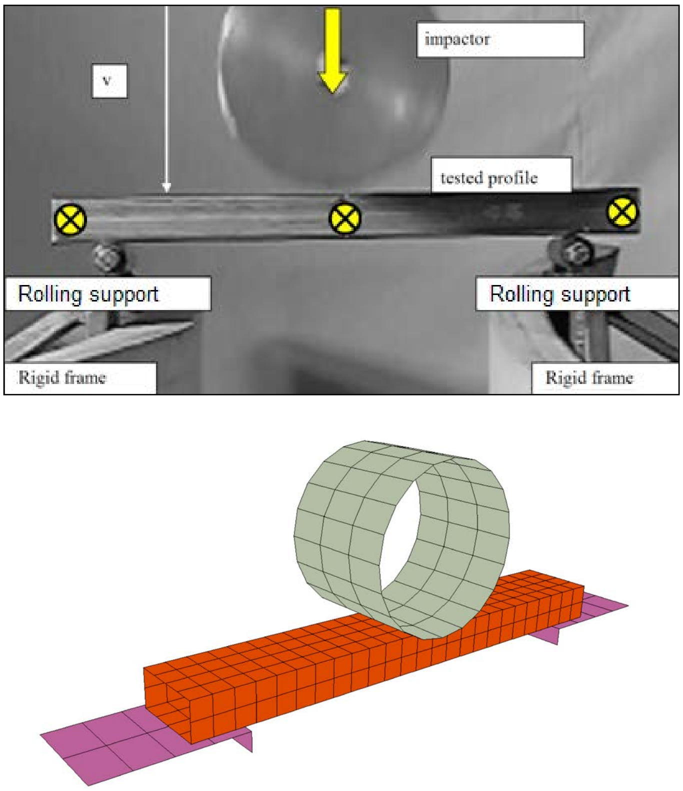

FIGURE 4: Drop test physical and virtual representation
OBRÁZEK 4: Pádová zkouška fyzická a její virtuální reprezentace

drop test is performed on the characteristic piece of window pillar that the impactor strikes. The impact energy during the test corresponds to the energy in the real test of the entire bus. In the PAM-Crash simulation software, this test is then replicated and based on the deformation evaluation using the video sequence, the numerical model is validated for the drop test.

In the case of small buses, the drop test is applied for more complex parts of the structure. These can, for example, be stamped parts, parts made by hydroforming etc. An example of the drop test for a bus A-pillar of is shown in Figure 5. It should be noted that the evaluation and subsequent tuning of the properties of a material model is more complex because deformations occur in several directions. In this case the deformations are measured using 2D tracking points, and plastic deformation is measured after impact by photogrammetry. For validation it is necessary examine the pillar behavior using video footage from a high-speed camera.

The creation of a numerical bus model is very time-consuming. It takes one full-time employee about four weeks to prepare a finite element (FE) model of an 18m long bus, and another two weeks is spent connecting and setting up the model.

In terms of computational time saving, a 3D CAD model that includes volume geometries is converted to mid-surface and the thickness is assigned to 2D elements only computationally. For computation purposes, 2D shell elements are used with five integration points using the Bellytschko-Tsay uniform reduced integration method. For steel materials, material model type 103 is used – Elastic Plastic Iterative Hill with Krupkovsky Law coefficients. A 3D model also contains a number of radii and holes unnecessary for R66 testing. Holes with diameter smaller than 1/5 of the smallest edge are removed and replaced by a mesh (elements), as are radii smaller than 1/5 of the smallest edge.

Welded joints are largely represented by coincident mesh nodes. This representation method is sufficient and creates smaller strain concentrators than other types of entities. In cases where the direct connection of mesh nodes cannot be used, the welds represent the entity characteristic of PAM-Crash, Plink. For predictable results on all models it is necessary follow the mesh quality and element sizes of the validation model. On parts belonging to the main structure, such as pillars, we use an element size of 8mm, which offers an acceptable combination of size (in terms of computation time) and accuracy. The internal criterion for minimum element length is 5mm for a model consisting of under 1 million elements. It is necessary to keep as many QUAD elements as possible in order to reduce stress concentrators, which are produced by inconsistent mesh with bad quality elements.

When the model is prepared, initial conditions and non-structural masses are added together with the mass balance with respect

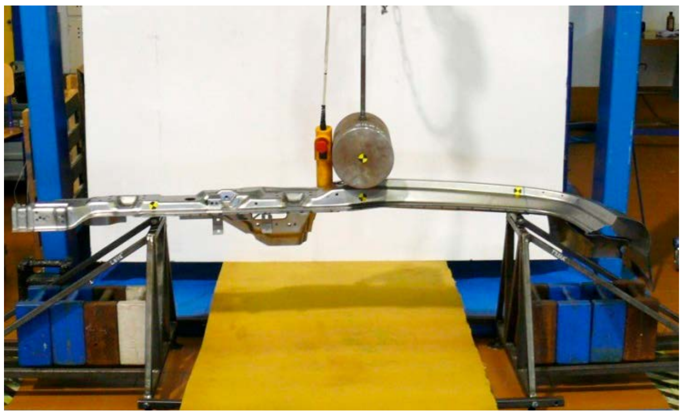

FIGURE 5: Drop test of an A-pillar
OBRÁZEK 5: Pádová zkouška A sloupku

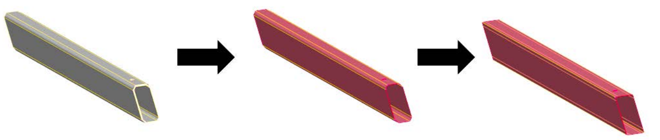

FIGURE 6: Pillar FEM model preparations
OBRÁZEK 6: Příprava MKP modelu sloupku

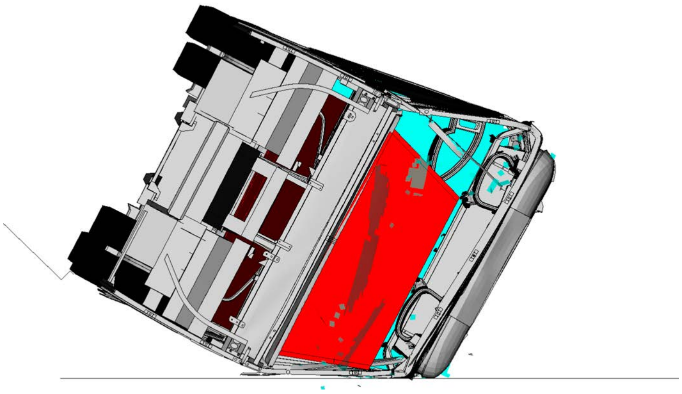

FIGURE 7: Bus rollover
OBRÁZEK 7: Převrácení autobusu

to the center of gravity. The position of the center of gravity in the Y and Z direction is very important for the simulation. It determines the unstable position when the platform is tilted. From the center of gravity values, this unstable position can be calculated and then the impact angular velocity determined. The accuracy of results is given by the impact kinetic energy of the model calculated from the moment of inertia and angular velocity. The evaluation of the R66 test is rather straightforward. If any part of the internal structure penetrates the survival space, the test is unsuccessful and structural changes are required.

4. CORRELATION PROCESS

To evaluate the results of the numerical simulation, the validation of partial results is necessary. These validations are performed as the numerical model is being created. Individual components are tested both quasi-statically and dynamically as indicated beforehand. One of the purposes of validation is determination of a suitable method for creating a mesh when connecting beams with different cross sections. The purpose, for example, of T-joint weld connections is to find an adequate simplified weld representation. These connections

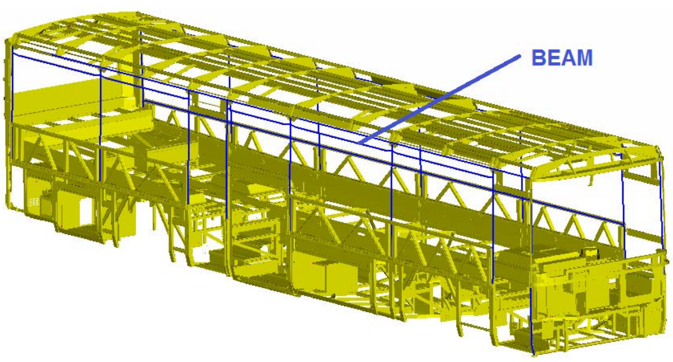

FIGURE 8: T joint with variable pillar height and difference between the PLink joint and connecting of adjacent nodes
OBRÁZEK 8: T spoj s proměnnou výškou profile a rozdíl mezi spojením typu PLink a napojení sousedních uzlů

are difficult for the numerical model due to the problematic joining of coincident nodes.
The most obvious variation of homologation simulation results is the physical examination of the bus segment. The segment must represent the main structure of the bus chassis, where the R66 test is performed. The most important result is the measurement of the maximum as well as plastic deformation, together with the determination of plastic joints and cracks. The deformation of an entire segment is measured with potentiometers located at the important points of the construction. From these measured points the deformation is evaluated. Tests are also captured with high-speed cameras, from which it is possible to determine the behavior of the test sample and deformations are evaluated using a photogrammetric method (2D). Accelerometers and other devices can also be used for validation, but this is optional and not every project definition requires such a detailed approach. One of the specialized measurements is, for example, strain gauges placed on washers for the measurement of axial forces in the bolts. These washers are calibrated for axial loads on the tensile test.

5. SIMULATION TEST PARAMETERS AND MEASUREMENT UNCERTAINTIES

Physical and virtual test results may be a little different due to model uncertainties. If we include all the model uncertainties of the virtual process and the physical validation, we obtain a total uncertainty in the region of ~ 20%. Some uncertainties are caused due mistakes in physical measurement and some come from numerical errors during computation. For example, a slight uncertainty is derived from running the computation on separate processors (parallelization) where each processor has an uncertainty in rounding. So, if computation is split between several processors, it can happen that a slightly different result is obtained with the same simulation. From experience, results from models prepared and validated in PAM-Crash software are slightly more conservative and show worse results when compared to the physical tests. In the case of homologation calculations, we are on the conservative, i.e. safe side. The calculation results are very dependent on several basic parameters, such as mass, position of the center of gravity, vehicle moment of inertia and impact velocity. There are also many other numerical parameters. Among these parameters are, in particular, the coefficient of friction between impact area and tested model. The coefficient of friction must be measured for a specific impact area and given in the technical protocol. Figure 9 shows differences between friction coefficients. The Y axis indicates the distance of the B pillar from the survival space template. With the improved friction coefficient of real concrete and steel (red line) there is greater deformation – it comes closer

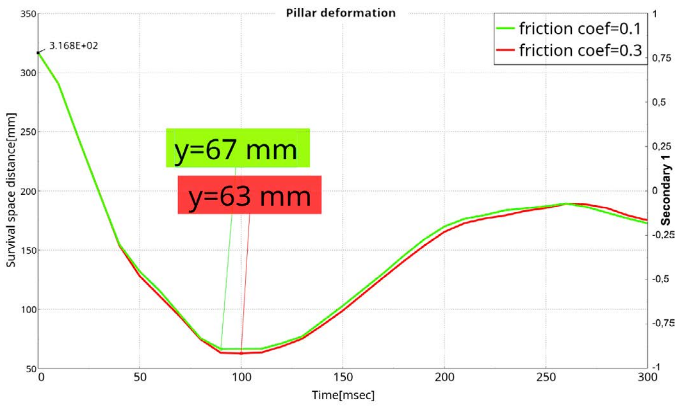

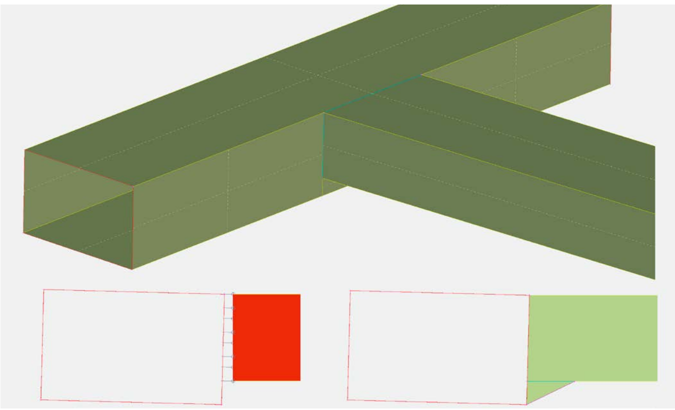

FIGURE 9: Distance of survival space template and B pillar in relation to friction coefficient
OBRÁZEK 9: Graf vzdálenosti prostoru pro přežití a B sloupku v závisloti na třecím koeficientu

FIGURE 10: Illustration of physical test validation
OBRÁZEK 10: Korelace fyzického testu a virtuální simulace

to the survival space template. Also, the friction coefficient changes the behavior of the whole rollover.
Boundary conditions are set according to the ECE R66 regulation. This means that applied to the model is gravitation and initial angular velocity. The simulation doesn't run through the whole rollover, but computation starts a few centimeters before first contact with the ground. Initial conditions are calculated from the unstable position.

6. CONCLUSION

Based on correlations between the physical tests and virtual simulations, the Czech Accreditation Institute (ČIA) acknowledged the internal methodology and subsequently accredited the Department of Virtual Simulations of TÜV SÜD Czech for the virtual testing of bus constructions according to R66. TÜV SÜD Czech performs about 15 virtual and 5 physical tests per year. There also remains great interest in the testing of entire buses. These tests have moved from pure homologation tests more to validation FE analysis, and are supporting the manufacturer's R&D department. The requirements for measurement equipment and post processing have increased, due to increased test complexity. In conclusion, however, it is important to note that progress in virtual testing has increased, but it still cannot completely replace physical testing. The best option for the testing departments, and also for the customer, is a suitable combination of both approaches. Final homologation can be achieved faster, more effectively and with lower cost. The bus design can be optimized and adapted to load conditions while maintaining all other operating parameters.

ACKNOWLEDGEMENTS

Presented results and procedures had been done with financial support of Technology Agency of Czech Republic in framework of project of Jozef Božek competence centre, Work Package 23 (WP23) respectively. Results of WP23 had been obtained in tight collaboration with Faculty of Mechanical Engineering at ČVUT, Department of Automotive, Combustion Engine and Railway Engineering and Department of Mechanics, Biomechanics and Mechatronics.

REFERENCES

[1] ČERNÝ, Ladislav. Bezpečnější autobusy. Auto Profi. 2017, 25(Červen), 1.
[2] TRUBAČ, Jiří. Analýza komplexnosti modelu na vyhodnocení pevnostní konstrukce autobusů. Praha, 2013. Bakalářská. ČVUT.
[3] SENTHIL KUMAR, D. Rollover Analysis of Bus Body Structure as Per AIS 031/ECE R66. Dostupné z: http://www.altairatc.com/india/previous-events/2012/papers-2012/RNL-A-07_Rollover_Analysis_of_Bus_Body_Structure_Volvo.pdf
[4] DVOŘÁK, František. Patrové autobusy by se měly zakázat, říkají odborníci na bezpečnost [online]. Dostupné z: https://auto.idnes.cz/patrove-autobusy-by-se-mely-zakazat-rikaji-odbornici-na-bezpecnost-1fy-/automoto.aspx?c=A110718_135127_automoto_fdv

10.1515/mecdc-2017-0003

JOINT SHAFT TEST STAND

JIŘÍ PAKOSTA, GABRIELA ACHTENOVÁ
CTU in Prague, Faculty of Mechanical Engineering, Department of Automotive, Combustion Engine and Railway Engineering
jiri.pakosta@fs.cvut.cz, gabriela.achtenova@fs.cvut.cz

ABSTRACT
The article focuses on description of design of the test stand for shafts with universal joints and constant velocity joints. The shafts can be loaded by torque at specified speed of rotation, while retaining the possibility of setting a variable angle between input and output. All shafts are instrumented with contactless signal transmission. In addition, ventilator simulates the cooling derived from the driving speed.
KEYWORDS: HOOKE'S JOINT, CV-JOINT, TEST STAND

SHRNUTÍ
Článek popisuje zkušební stav pro měření kloubových hřídelů. Hřídele mohou být zatěžovány točivým momentem při různých otáčkách a měnícím se úhlu zlomu. Měřené hřídele jsou vybaveny snímaním teploty kloubů s telemetrickou soupravou přenosu signálu. Klouby jsou chlazeny náporovým ventilátorem, který simuluje ochlazování kloubů při jízdě vozidla.
KLÍČOVÁ SLOVA: KŘÍŽOVÉ KLOUBY, HOMOKINETICKÉ KLOUBY, ZKUŠEBNÍ ZAŘÍZENÍ

1. INTRODUCTION
Joint shafts of drive axles are increasingly used types of wheel drives in passenger automobile drive trains. In steerable drive axles, constant-velocity joints are the only way how driving power can be transmitted to the driving wheels in a conventional drive train with a combustion engine. Thorough description of used types, their design and calculation can be found in [1]. Brief overview of joint shaft is covered in [2].

Great progress can be seen recently in the area of creation of virtual prototypes where the product designed is replaced with a computer simulation model. The virtual prototype tries to verify the in-service behavior of the real product without having to manufacture it. The virtual prototype is created using mathematic modeling methods which cover stress-strain and dynamic analyses, heat transmission, flow dynamics, acoustics, and a number of other physical processes. Each mathematic model, however, is based on simplifying hypotheses which only approximate, to a greater or lesser extent, the actual solution, and much of the input data for the mathematic model is obtained through experiments using simplified realistic models. The mathematic models thus reduce the required number of test prototypes manufactured, although they do not eliminate the need for them entirely. Therefore production of realistic prototypes and testing equipment for testing new components is still important today and is covered in this article. The article describes the newly created test stand for testing of joint shafts in the laboratories of the Department of Automotive, Combustion Engine and Railway Engineering.

2. TEST STAND CONCEPT
In order to use the test stand to simulate the actual behavior of drive shafts in a vehicle as accurately as possible, the stand must imitate the operating conditions as much as possible. In addition, it must include a number of sensors for automation, diagnostics and evaluation of the test. The stand should serve for tests of joint shafts with universal joints as well as shafts with constant velocity joints. As the majority of passenger vehicles are designed with transverse power unit and front axle drive where the use of constant velocity joints is inevitable, the stand was set up and primarily tested for the tests of these shafts.

The operating conditions are defined by the torque at specified speed (rpm) and the set bend angle. The joint shaft is loaded

with the driving or braking torque between the engine and the transmission gear and the wheel of the vehicle. The rotation speed of the joint shaft is directly proportional to the driving speed of the vehicle. The bend angle ranges between its minimum and maximum design value.
The test stand can be designed as an open or closed test stand. A closed test stand has the advantage consisting of lower energy demand of long-term tests, but its closed space design significantly complicates the tests of various lengths of jointed shafts and a broader range of the bend angles. Therefore an open test stand has been selected as a test stand concept.

3. OPEN TEST STAND FOR JOINT SHAFT TESTING

The open test stand consists of the input drive dynamometer which is controlled to constant torque, and the output dynamometer controlled to constant rotation speed. The scheme of the stand is depicted on Figure 1. The input dynamometer is placed on the profile rail linear guide in longitudinal direction (in the direction of the dynamometer axis). This dynamometer is a two shafts asynchronous dynamometer. The eddie current output dynamometer is placed on linear guide system in transverse direction (perpendicular to the dynamometer axis). This linear guide system consists of a pair of rails and four ball-bearing carriages. The rails are attached with fasteners to the base plate of the testing site; the ball-bearing carriages are attached with screws to the dynamometer frame. Positioning of the dynamometers is facilitated by the use of screw jacks controlling the mechanism of the lead screws. The main parameters of both dynamometers are listed in Table 1.

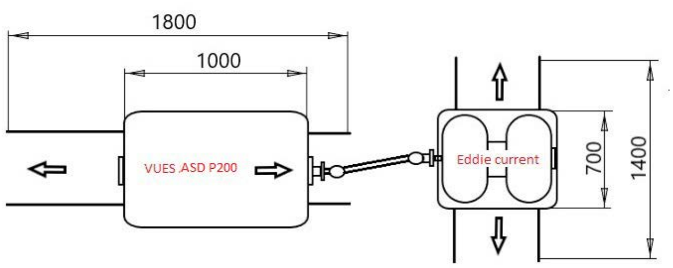

FIGURE 1: Scheme of the set-up for joint shaft experimental testing
OBRÁZEK 1: Schéma stavu pro zkoušky kloubových hřídelů

The position of the shaft in the vertical axis direction in the output dynamometer can be easily set by insertion of calibrated washers between the supporting frame and the dynamometer itself. This resulted in a universal station with the following characteristics:

- Easy and quick adjustment to different lengths of the joint shafts
- Easy change of the bend angles of the shafts.

If the axis of the movable dynamometer is set at the same height as the axis of the fixed dynamometer the subsequent setting of the bend angle only takes place in-plane, which makes the operation of the stand easier.

TABLE 1: Dynamometer parametres
TABULKA 1: Parametry dynamometrů

Parameter	Input dynamometer	Output dynamometer
Type	Asynchronous	Eddie current
Specification	ASD P200	2VD110/6
Maximal rpm	7000 rpm	6000 rpm
Maximal torque [N.m]	1100	800
Maximal power [kW]	200	220

The stand is designed such that the axes of the dynamometers are parallel. It is therefore possible to test joint shafts with universal joints with "Z" and "V" bend configuration or, as the case may be, layout with the same space angles. If testing of the joint shaft layout with different joint angles is needed it is possible to deviate the axis of rotation of the output dynamometer to the space. Such configuration, however, would substantially complicate the set-up of the bend angles during the tests.
The bend axis is changed by the motion of the dynamometer in transversal axis. Dependence of the magnitude of the travel on the value of the bend angle is determined by the trigonometric function of transversal displacement of output dynamometer divided the length of the joint shaft. When testing constant bend angles of a joint shaft, it is possible to fix the dynamometer frame to the rail by pneumatically released friction brake. In tests with the changing bend angle, it is possible to drive the screw jack with programming capability using an electric motor.
In order to move the dynamometer during operation it was necessary to provide flexible lines of power supply, pressurized air, coolant and sensor conductors. For cooling of the joint shafts, the stand is additionally equipped with fans the cooling effect of which can be adjusted by the distance from the joint shaft or the value of the fan propeller rotation speed.
When driving in a vehicle, each joint is blown at by a different air flow. The joint on the gearbox side is typically "shielded" by the shape of the gearbox while the joint on the wheel side is cooled by air with substantially higher velocity. The velocities of the air blowing at each joint have been obtained from the vehicle manufacturers. In laboratory testing, where the joint

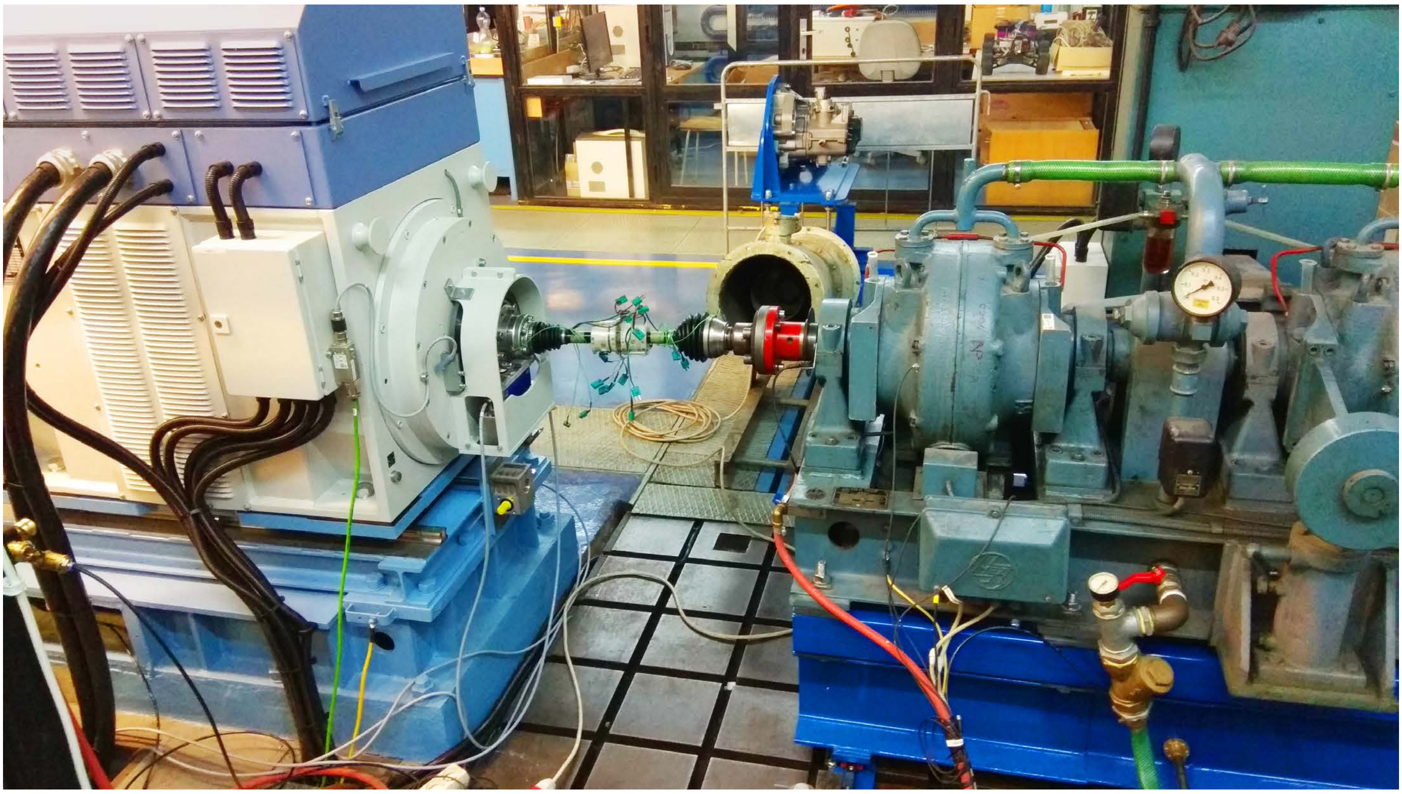

FIGURE 2: Open test stand for testing of joint shafts
OBRÁZEK 2: Otevřený zkušební stav pro zkoušky kloubových hřídelů

shaft is attached with screws directly to the dynamometer flanges, the following solutions are possible:

1. Using two fans of different parameters
2. Using a fixture for shielding a part of the airflow for the "gearbox joint",
3. Correct positioning of the fan such that greater amount of air would flow to the "wheel" joint.

We have opted for the third solution. The correct position of the cooling fan was determined by means of anemometric measurement of the velocity of the air blowing at the two joints. The final position was fixed in order to ensure repeatability of the measurement.

4. MAGNITUDES MEASURED

The value of the required load torque is set on the input dynamometer. The load torque corresponds to the one half of the driving torque of the vehicle needed to propel the vehicle on given constant speed on straight flat road. As example we assume the speed of the vehicle equals 175 km/h; the needed torque on one driving wheel equals 248 N.m. The torque measured on the output dynamometer is lower due to the efficiency of the joint shaft. When testing constant-velocity joint shafts, the input and output rotation speed is the same. The necessary speed of rotation n is defined from the given vehicle speed v with help of the dynamic radius of the tire r. The test parameters obtained for the mentioned assumption are listed in Table 2.

$$n = \frac{v}{2\pi\, r}\,\frac{1000}{60} \tag{1}$$

The devices suitable as joint temperature sensors are, due to their minimal dimensions, thermocouple thermometers which are placed in drill holes in the joint body. Signal transmission from the rotating shaft is contactless. In addition, the measuring apparatus attached must be balanced in order to avoid additional load on the joint shaft measured.

TABLE 2: Example of test parameters
TABULKA 2: Ukázka zkušebních parametrů

Run-in torque for a bend angle of 7°	50 N.m
Time of run-in	0,5 h
Test load torque	248 N.m
Time of one measuremeng	0,57 h
Rpm of one half shaft	1441 rpm
Tested bend angles	7°, 8°, 9°a 10°

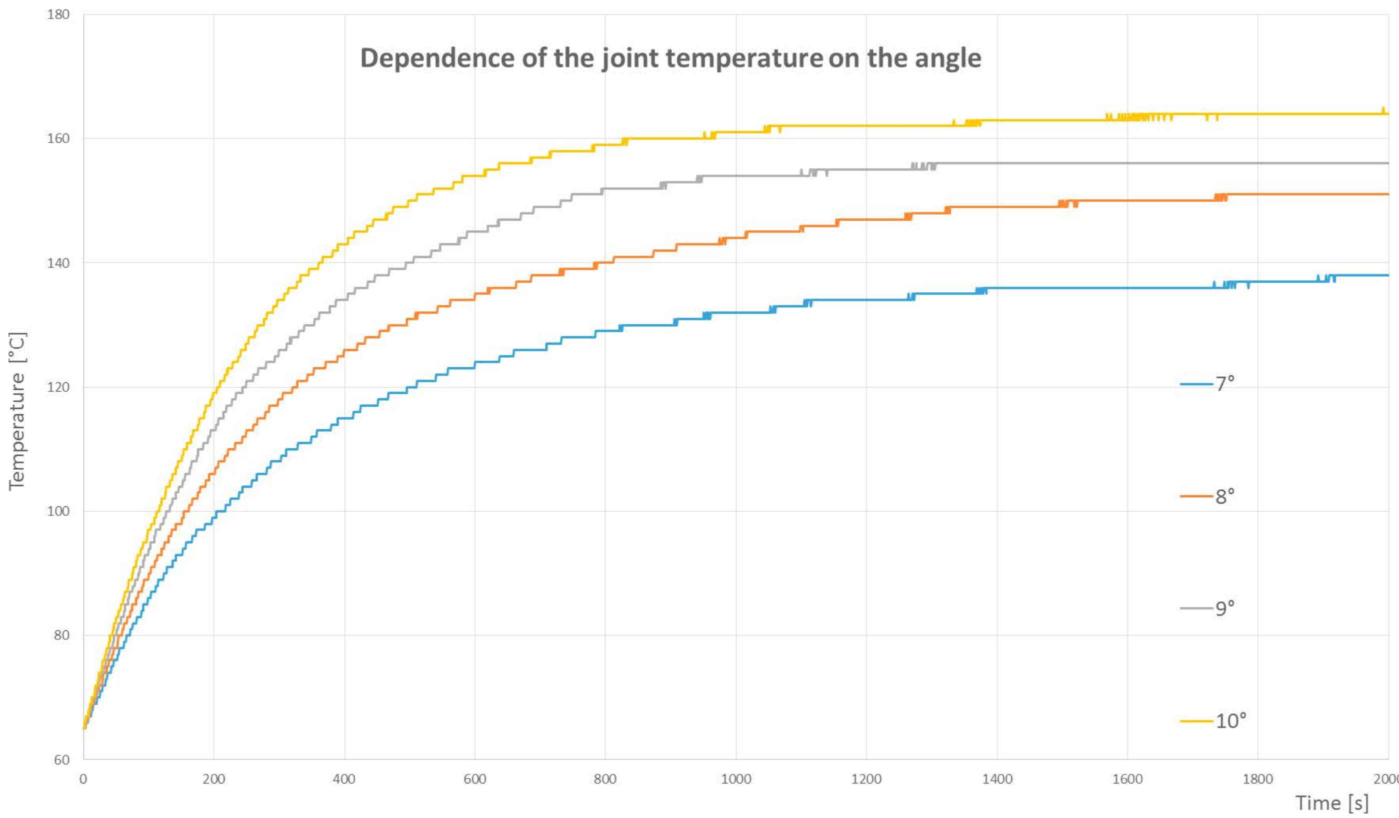

FIGURE 3: Dependence of the temperature of one selected CV joint of the automotive joint shaft on the bending angle.
OBRÁZEK 3: Závislost nárůstu teploty na úhlu zlomu u zkoušeného kloubového hřídele

Various measurements can be performed in the test stand, from functional tests up to lifespan measurements. In the present case, we measured dependence of the joint temperature on the changing bend angle. For one torque and speed level we measured the temperature dependence on the bend angle in most of the operating range of the joint shaft. The joints were cooled down to the original temperature between the individual measurements. The time of the measurement is determined as the necessary time needed to drive with a given speed v the distance of 100 km. For the speed of 175 km/h the measurement time equals 34,2 min. A sample of the temperatures measured during the test defined in Table 2 is depicted on Figure 3.

5. CONCLUSION

The correct design of the stand with mounting of dynamometers on linear sliding system was affirmed as fully functional by a test of different joint shafts focusing on the measurement of the increase of temperature of the joints depending on the changing bend angle. The test stand can be further equipped with the rotary encoder to obtain the value of non-uniform rotation of the joint shafts. As next is investigated the possibility of precise torque measurement to be capable to measure the efficiency of the joint shafts. This measurement with the nowadays equipment is not possible.

ACKNOWLEDGEMENT

The authors would like to thank Škoda Auto, a.s. for provision of joint shafts, and for lending the unique system for measurement of temperatures of rotating shafts.
This research has been realized using the support of The Ministry of Education, Youth and Sports program NPU I (LO), project # LO1311 Development of Vehicle Centre of Sustainable Mobility.
Both supports are gratefully acknowledged.

REFERENCES

[1] Graf can Seherr_Thoss H. CH.: Gelenke und Gelenkwellen. Springer Verlag. 2002. ISBN 3-540-41759-1.
[2] Achtenová G., Klír V.: Převodná ústrojí motorových vozidel. Kloubové hřídele. CTN – nakladatelství ČVUT. 2012. ISBN 978-80-01-05129-0

DE GRUYTER OPEN

10.1515/mecdc-2017-0004

IDEAS FOR TESTING OF PLANETARY GEAR SETS OF AUTOMOTIVE TRANSMISSIONS

GABRIELA ACHTENOVÁ
Czech Technical University in Prague, Faculty of Mechanical Engineering, Technická 4, Prague 6, gabriela.achtenova@fs.cvut.cz

ABSTRACT
The article describes the concept of modular stand, where is possible to provide tests of gear pairs with fixed axes from mechanical automotive gearboxes, as well as tests of separate planetary sets from automatic gearboxes. Special attention in the article will be paid to the variant dedicated for testing of planetary gear sets. This variant is particularly interesting because:
1) it is rarely described in the literature, and
2) this topology allows big simplification with respect to testing of standard gearwheels.
In the planetary closed-loop stand it is possible to directly link two identical planetary sets. Without any bracing flange or other connecting clutches, shafts or gear sets, just two planetary sets face-to-face will be assembled and connected to the electric motor.
KEYWORDS: **CLOSED-LOOP TEST STAND, EFFICIENCY OF PLANETARY SET, ENDURANCE TESTS**

SHRNUTÍ
Článek popisuje koncept modulárního zkušebního stanoviště, kde je možné testovat jak ozubené převody s pevnou osou, tak planetová soukolí. Zvláštní pozornost bude v článku věnována právě zkoušení planetových převodů. Tato varianta je zajímavá z několika důvodů:
1) je velmi málo popsána v literatuře,
2) uspořádání umožňuje velké zjednodušení v porovnání se stavem pro soukolí s pevnou osou.
V zkušebním stavu planetových soukolí je možné napřímo spojit dvě identická soukolí. Bez jakých koli přídavných spojek, hřídelů, nebo dalších převodů. Máme pouze dvě propojená soukolí, které jsou přímo poháněny elektromotorem.
KLÍČOVÁ SLOVA: **UZAVŘENÝ ZKUŠEBNÍ STAV, ÚČINNOST PLANETOVÝCH PŘEVODŮ, ŽIVOTNOSTNÍ ZKOUŠKY**

1. INTRODUCTION
The physical testing of gearboxes, despite the quick development of simulation methods, remains a very important part of the design process. The main target is to determine the functional properties like efficiency, noise, vibrations, and endurance. The paper will be focused on closed-loop test stand. Big advantage of the closed-loop test stand is the possibility to build a cheap experimental device, which allows large range of experiments. Apart from endurance tests (typical for such device thanks to low energy demands) it will also be possible to measure transmission error, non-uniform load distribution on planets, vibrations and other parameters.
The idea to test gear wheels or whole gearboxes in a closed loop stand is generally attributed to Prof. Niemann [1]. The load is raised by elasticity forces when distorting the shafts with help of bracing flange and torque arm with weights. The load circulates in the whole test stand. The power from the motor is used only to compensate the losses in the stand. Two identical gearwheels (gearboxes) are necessary. One is called tested gearbox, the other technological gearbox. The technological gearbox rotates the opposite sense of rotation. The load torque enters the technological gearbox via the output shaft. The opposite sense of rotation combined with opposite torque flow implies that in both gearboxes the same teeth flanks are loaded. For the gearwheels we can obtain two results from one endurance test. The technological gearbox is loaded with a torque diminished by efficiency of the previous parts of test stand.
As mentioned in previous paragraph the idea of the closed-loop testing is well-known for many years, and is widely used. Universities [2], [3] and research companies dealing with research and development of gearwheels are equipped with such test stands. They are using in-house stands, or standard test machine manufactured by e.g. StramaMPS Maschinenbau GmbH [4]. The disadvantage is that most of the stands are dedicated for

spur gears only; the gearwheel axis distance is approximatively 90 mm, which is too much for automotive gearbox.
The mechanism of closed-loop test stand can be simplified if planetary gearsets will be used. Prof. Šalamoun [5] introduced the idea of usage of closed loop test stand for testing of planetary gearboxes. The test stand was newly built in laboratories of Czech Technical University in Prague. The concept, design and first results are presented in this paper.

2. CLOSED LOOP STAND FOR PLANETARY GEAR SETS

There is a huge variety of composition of planetary sets. Typically in automotive gearboxes the mostly used sets are with central wheels (one sun and one crown wheel) with a single simple planet. The gearboxes with positive base ratio (with two planets) or with Ravigneaux set are relatively exceptional. Therefore we decided to start the test stand with the mostly used set with negative base ratio. The parameters of the planetary sets are mentioned in Table 1. To use the real gear sets from the automotive transmission we disassembled the sets from two identical automatic transmissions. The scheme of the stand can be seen in the following Figure.
Different solutions for different types of gear sets are elaborated in [6]. To be able to test different types of planetary sets the casings and their bearing houses are designed slightly over-dimensioned. The following chapter is dedicated to description of the realized test stand.

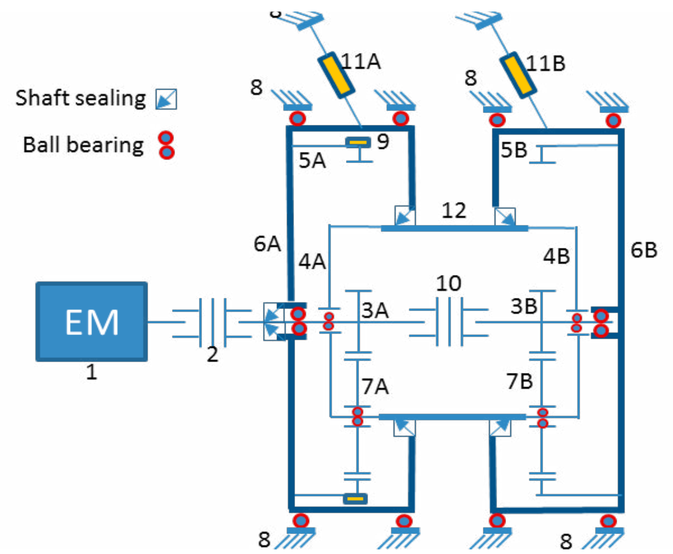

LEGEND: 1 – Electric motor, 2 – Stiff bellow clutch with clamping hub, 3 – Sun Gear, 4 – Spider, 5 – Crown wheel, 6 – Planetary set casing, 7 – Planet, 8 – Frame, 9 – Strain gauges, 10 – GE-T Coupling with flexible spider, 11 – Sensor of reactional force, 12 – Tube connecting spiders 4A and 4B, A – Belonging to gearbox A, B – Belonging to gearbox B

FIGURE 1: Scheme of the new test stand for planetary gear sets
OBRÁZEK 1: Schéma nového stavu pro zkoušky planetových soukolí

TABLE 1: Parameters of the tested planetary sets
TABULKA 1: Parametry použitého planetového soukolí

Element	Sun	Planet	Ring wheel
Number of teeths	31	22	74
Base ratio		$i^r = -2{,}3871$	

There are two possibilities how to introduce the preload into the circuit:

- Preload of reactional member (in Figure 1 it can be realized by preloading of one of the crown wheels. The torque can be changed any time.
- Distortion of shaft linking suns or spiders (in Figure 1 for example coupling 10 could be exchanged by bracing flange, when mounted externally from sets). The torque can be changed in steady state only.

With regard to the simplicity of the solution and with regard to the possibility of change the load any time we decided to use the first option of preload.

3. REALISED TEST STAND

The tested planetary sets are depicted in Figure 2. The four speed gearbox, from which we took the PGS consisted of two nested planetary sets with common sun; therefore the sun gearwheel is wide. The gear of the sun is manufactured directly on the hollow shaft, which is on one extremity equipped with splines. The crown wheel is a thin ring, which will be later equipped with strain gauges for measurement of non-uniformity of planet loading. The crown wheel is rigidly connected to a splined flange and with respect to the sun is connected via ball bearing. The spider holds three uniformly distributed planets. The spider is welded part. Between spider and sun is placed a ball bearing. For the connection of spider with the spider of the second planetary set are dedicated 6 dogs.
Every planetary set is enclosed in the circular casing, which is mounted on two ball bearings. The casing has to be mounted free in rotation, to give the possibility to measure the reactional force on the casings, i.e. the reactional force on the crown wheel. Next reason is that the preload into the circuit is introduced via loading of one reactional element, i.e. via loading of one casing.
The spiders are linked together via rigid hollow tube. The suns are connected together via the flexible coupling. To clearly distinguish between both sets, we will introduce the following notation: the PGS linked with the electric motor is called "A", the PGS where the load is introduced is called "B". In the sun gear of PGS A was pressed the shaft which is via bellow coupling connected to the electric motor. The electric motor rotates the whole stand and compensates for the losses. The electric motor is controlled by frequency converter; the parameters are stated in the following table.

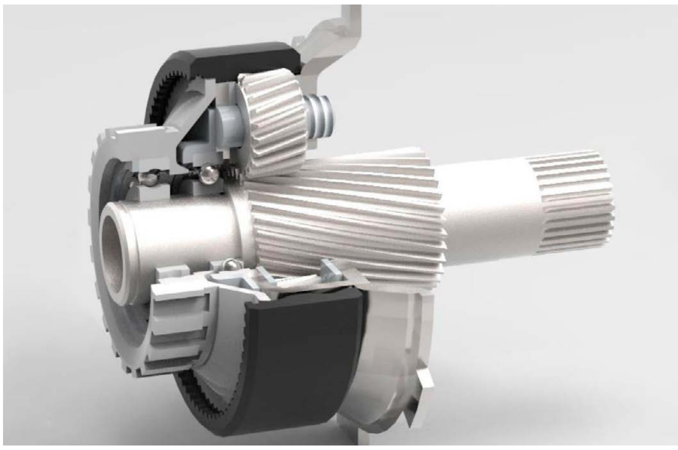

FIGURE 2A: Vizualisation of the cross section of the tested planetary gear set; [7].
OBRÁZEK 2A: Vizualizace řezu planetovým soukolím; [7].

FIGURE 2B: Photo of the PGS; [7].
OBRÁZEK 2B: Fotografie planetového soukolí; [7].

TABLE 2: Parameters of electric motor
TABULKA 2: Parametry elektromotoru

Electric motor	n_{max}	P_{max}	$M_{nominal}$
ABB M3EB 100E6	6400 1/min	18 kW	43 N.m

The section of the assembled closed-loop planetary stand is depicted in Figure 3. Figure 4 shows the visualization of assembled stand. From Figure 4 can be clearly seen, that one planetary casing is mounted on the linear rail in axial direction of the PGS (to facilitate the final assembly), one planetary casing is mounted on the subframe, which can be transversally manipulated to achieve perfect alignment of both planetary sets. The final grinding of both frames of planetary sets was done at once, to ensure the alignment in vertical direction.
The lubrication is proposed as churning, in the future pressure lubrication will be designed. Every casing has oil inlet and outlet connection socket, as well the draining tap. For the tested PGS's there is no sealing between sun and spider, so the oil can partly fill the tube (12) connecting the spiders.
The preload is introduced via flange (9), which is screwed to the casing (2), sealed with o-rings. The flange is equipped with dogs, in which is introduced the counter dogs of load lever. The lever can be screwed to the flange (9), on the extremity of the preload lever are put the weights. The weights can be added or removed also during rotation of the stand, so the preload can be changed. The lever was designed as one side lever, only, so the change of loading torque is not possible – see Figure 4.

LEGEND:
1 – casing of PGS "A" linked with electric motor
2 – casing of the PGS "B"
3 – housing of ball bearing with axial fixation
4 – housing of ball bearing
5 + 6 – ball bearings supporting casings
7 – cover of spider sealing
8 – cover ensuring the axial fixation of bearing (6)
9 – flange for loading of PGS casing (2)
10 – cover with input shaft sealing
11 – input shaft
12 – tube connecting spiders
13 – flexible coupling connecting the suns
14 – spider sealing
15 – input shaft sealing
16 – circlip.

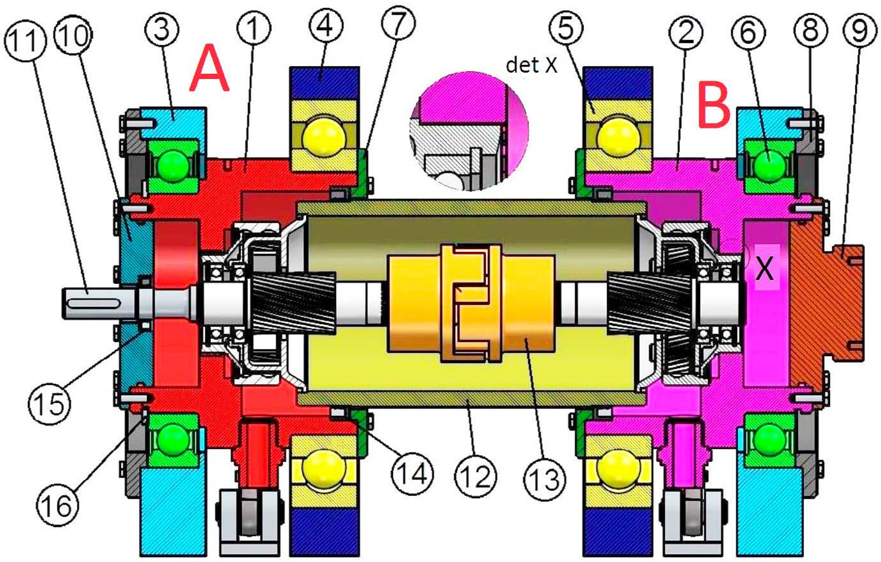

FIGURE 3: Section of assembled stand; [7]. The frames and sub-frames are not depicted.
OBRÁZEK 3: Řez sestaveným zkušebním stavem; [7]. Rámy a pomocné rámy nejsou znázorněny.

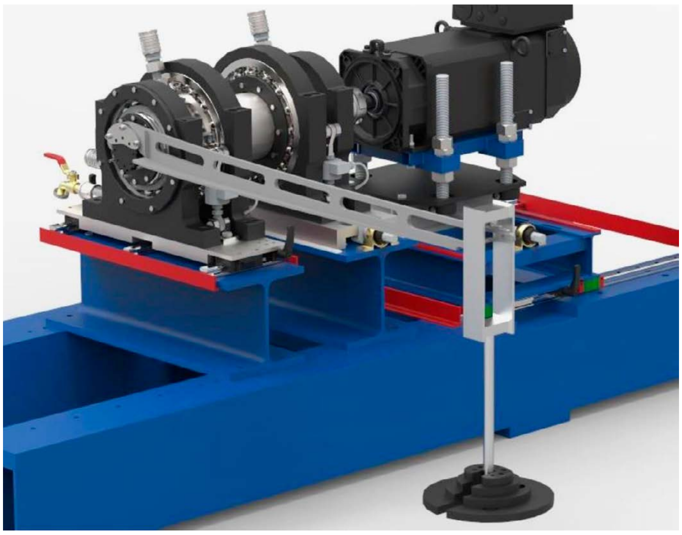

FIGURE 4: Visualization of the assembled test stand; [7].
OBRÁZEK 4: Vizualizace sestaveného zkušebního stavu; [7].

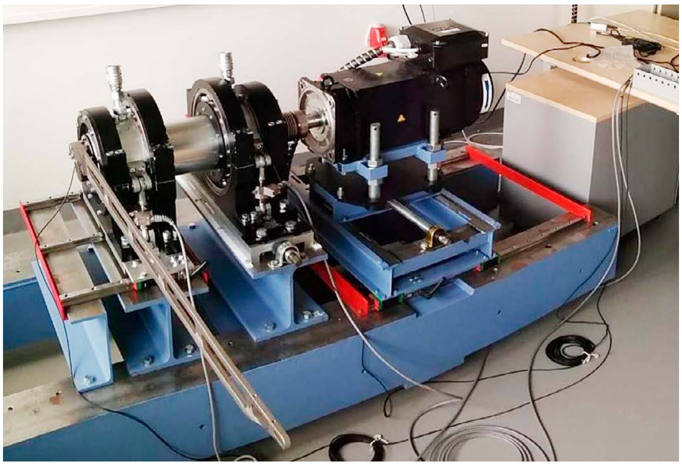

FIGURE 5:. Photo of the assembled test stand
OBRÁZEK 5: Fotografie dokončeného zkušebního stanoviště.

The reactional force is sensed with help of full-bridge strain gauge sensor HBM U2A with capacity of 1 t. The sensors are capable to measure the tensile and pressure force. Above the PGS bearings, on the casing are screwed the accelerometers KS77C 10. The information about speed of rotation is actually taken from the frequency converter. Since all elements are connected via gearwheels, the speed of rotation of remaining elements can be easily calculated.
The frame holding the electric motor is composed from several sub-frames. The sub-frame is mounted on linear rails to achieve easy movement horizontally in axial direction of electric motor. To facilitate the alignment with gearbox input shaft the sub-frame is equipped with positioning screw, which can tune the position in transversal direction. The smallest part of the sub-frame where the electric motor is screwed is mounted on four screws which ensure the position in vertical direction. As the stand is designed as modular – allowing the test of the fixed axes gearwheels as well as of the planetary sets, the easy and precise tuning of position of electric motor is important. For connection of electric motor with gearbox input shaft is used bellow coupling with clamping hubs.

4. POWERFLOW IN PLANETARY CLOSED LOOP TEST STAND

For planetary sets are in fact just two possibilities of the powerflow in the closed loop test stand, see Figure 6. The sense of circulating power depends on:

- The sense of the preload;
- Basic ratio of the PGS, and architecture of the tested PGS's;
- Sense of rotation and torque of the electric motor.

The determination of the magnitude of circulating power (torque) is more complex than in the case of closed-loop test stands for gearwheels (gearboxes) with fixed axes, where the preload is in fact the circulating torque; [8]. In case of planetary

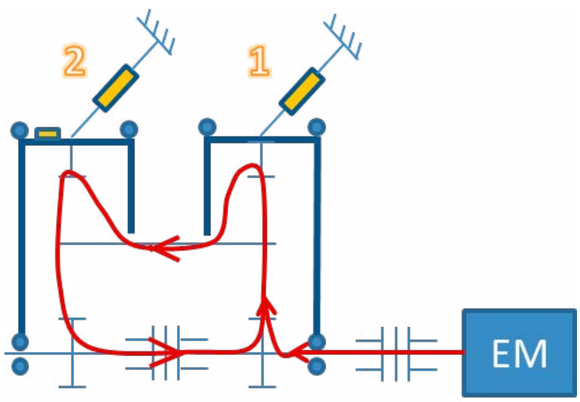

Case A) Power on Sun1 is positive.

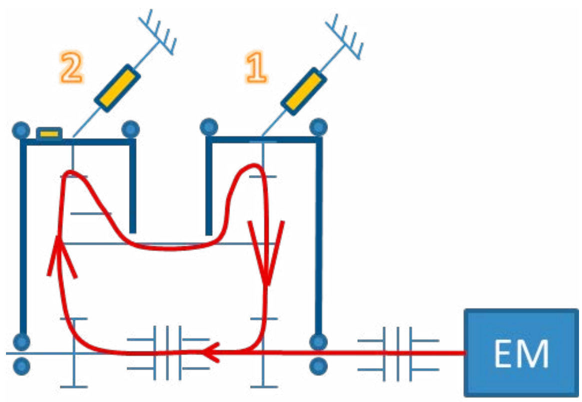

Case B) Power on Sun 2 is positive.

FIGURE 6: Two possible senses of the circulating power in the closed-loop test stand.
OBRÁZEK 6: Dva možné toky výkonu v uzavřeném zkušebním stavu

Case 1	Case 2
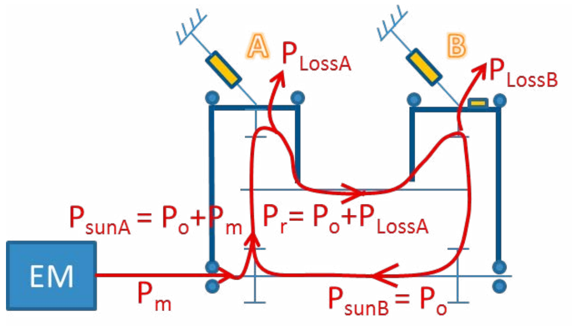	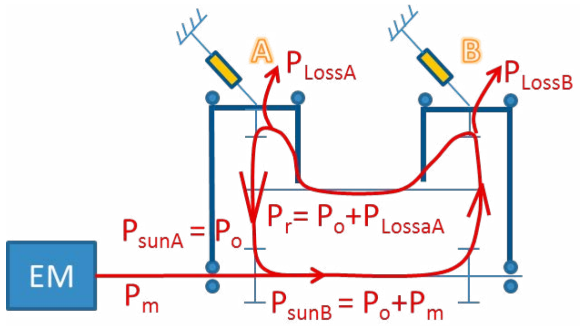
The equations of torque equilibrium	
$M_o = -M_{SunB}$	$M_o = -M_{SunA}$
$M_{SunA} = M_o + M_m$	$M_{SunB} = M_o + M_m$
$M_{rB} - M_{rA} = (M_o + M_m)\cdot i_A \cdot \eta_A$	$-M_{rB} = M_{rA} = (M_o + M_m)\cdot i_B \cdot \eta_B$
$M_{crownA} = (M_o + M_m)\cdot(i_A \cdot \eta_A - 1)$	$M_{crownB} = (M_o + M_m)\cdot(i_B \cdot \eta_B - 1)$
$M_{crownB} = M_{rB}\cdot(i_B \cdot \eta_B - 1) =$ $= (M_o + M_m)\cdot i_A \cdot \eta_A \cdot (i_B \cdot \eta_B - 1) =$ $= (M_o + M_m)\cdot \eta_A \cdot (\eta_B - i_A)$	$M_{crownA} = M_{rA}\cdot(i_A \cdot \eta_A - 1) =$ $= (M_o + M_m)\cdot i_B \cdot \eta_B \cdot (i_A \cdot \eta_A - 1) =$ $= (M_o + M_m)\cdot \eta_B \cdot (\eta_A - i_B)$
The equations of equilibrium of lost powers	
$P_{LossA} + P_{LossB} = P_m$	
$-P_{aA}\cdot(1-\eta_A) - P_{aB}\cdot(1-\eta_B) = P_m$	
$-(P_o + P_m)\cdot(1-\eta_A) - (P_o + P_m)\cdot\eta_A\cdot(1-\eta_B) = P_m$	$-(P_o + P_m)\cdot\eta_B\cdot(1-\eta_A) - (P_o + P_m)\cdot(1-\eta_B) = P_m$
Final equations taking into account the lost power (torque), efficiencies and circulating power (torque)	
$P_m = P_o \cdot \left(\frac{1}{\eta_A \cdot \eta_B} - 1\right)$ $M_m = M_o \cdot \left(\frac{1}{\eta_A \cdot \eta_B} - 1\right)$	
Ratios used in previous equations	
$i_A = i^{crownA}_{sun1.rA} = 1 - i^{rA}_{sunA.crownA} =$ $= 1 - (-2{,}3871) = 3{,}3871$	$i_A = i^{crownA}_{rA.sunA} = \frac{1}{i^{crownA}_{sunA.rA}} =$ $= \frac{1}{1 - i^{rA}_{sunA.crownA}} = \frac{1}{1-(-2{,}3871)} = 0{,}295$
$i_B = i^{crownB}_{rB.sunB} = \frac{1}{i^{crownB}_{sunB.rB}} =$ $= \frac{1}{1 - i^{rB}_{sunB.crownB}} = \frac{1}{1-(-2{,}3871)} = 0{,}295$	$i_B = i^{crownB}_{sunB.rB} = 1 - i^{rB}_{sunB.crownB} =$ $= 1 - (-2{,}3871) = 3{,}3871$

sets the preload is moment exerted on the reactional element. Firstly we will determine the powerflow and circulating power for both possible senses and then we will determine which case is relevant for our test stand.

4.1 POWERFLOW AND CIRCULATING POWER – GENERAL DERIVATION

To determine the magnitude of circulating power as well as the efficiency of planetary sets, we will write the equations of power and torque equilibrium. In the following Table can be seen the magnitude of powers on different elements. The appropriate equations are derived for both cases.

Before we will determine the equations valid for actual example, we will recall the definition of the lost power of any mechanism. The lost power can be determined with help of power on the input shaft, or of the output shaft.

$$P_{Loss} = -P_a \cdot \zeta = \frac{P_n}{\eta} \cdot \zeta \tag{1}$$

$$\eta \;=\; 1 - \zeta \tag{2}$$

We are measuring the total lost power, i.e. the power of electric motor, and the reactional moments, therefore it will be wise to carefully look on the equations of power and torque equilibrium.

4.2 POWERFLOW IN TREATED CASE

To determine the powerflow and magnitude of circulating power in our example, we will first treat the rotational speed, torque and power as algebraic values. We assume that the positive rotational speed and positive torque correspond with the sense of rotation and sense of torque of the electric motor. In such case the power of electric motor is also positive.

To determine the sense of circulating power, we have to first determine the sense of preload on the reactional element. We can simplify the calculation with neglecting the losses. We introduce the preload on PGS "B". The preload is introduced in the same sense as is the rotation and torque of electric motor. From the following calculation can be seen that the positive reactional torque can be obtained in Case 2 in Table 3 only.

$$\begin{aligned} &M_{preload} > 0 \\ &i_B = +3{,}3871 \\ &\overline{M_{rB}} = -i_B \\ &\overline{M_{crownB}} = -\overline{M_{sunB}} - \overline{M_{rB}} = -1 + 3{,}3871 = +2{,}3871 \end{aligned} \tag{3}$$

From the equation (3) can be seen that the positive reactional torque can be obtained only in case 2 – see Table 3.

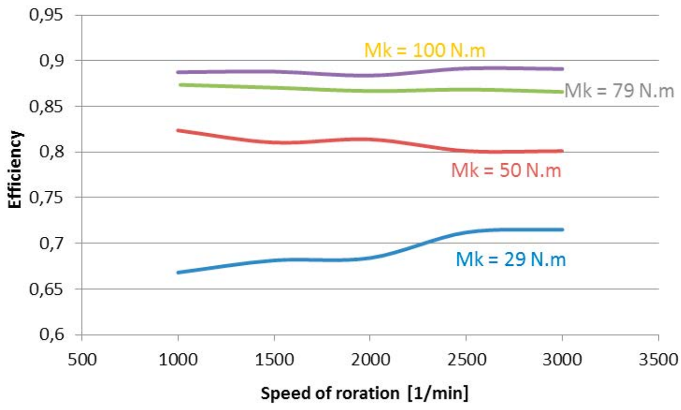

FIGURE 8: Dependence between efficiency and speed of rotation with respect to different preload on PGS B

OBRÁZEK 8: Závislost účinnosti na změně otáček vstupního hřídele a měnící se zátěži.

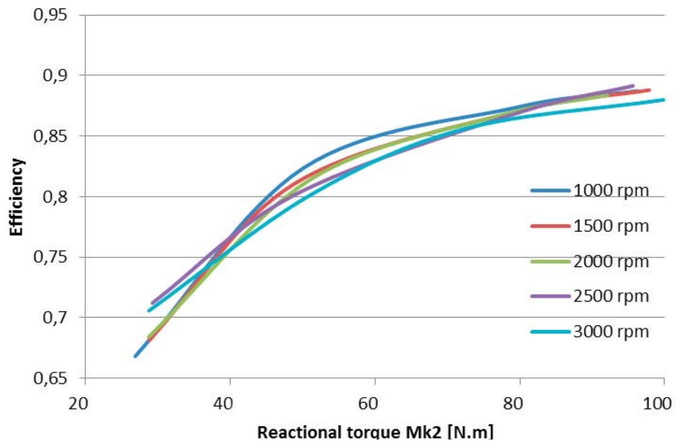

FIGURES 9: Dependence between efficiency and preload with respect to different rpm's.

OBRÁZEK 9: Závislost účinnosti na předpětí při různých otáčkách vstupu.

5. MEASUREMENT RESULTS

The measurement stand was recently built. Unfortunately the load cell on crown wheel "A" did not function well, so the results are from the reactional torque on crown wheel B only. It means we can not determine the efficiency of the PGS "A" and PGS "B" separately. For planetary gear sets with high efficiency, the difference of efficiency for power flow from sun to spider with fixed crown and of the efficiency for power flow from spider to sun with fixed crown, can be neglected. In our case we obtained relatively low efficiency, but the reason is mainly in the lubrication, i.e. in the churning losses.

In the following Figure can be seen the graphs from measured data. The measurements were done with different speed of rotation and different preload. The efficiency of PGS was calculated as well as the magnitude of circulating power and torque. The measurements were done with the oil temperature equal 35 C.

TABLE 4: Example of measured and calculated data.
TABULKA 4: Ukázka naměřených a vypočtených dat.

n [rpm]	P_m [W]	Mk2 [N.m]	M_m [N.m]	Efficiency	Mo [N.m]	Po [W]
3000	3104	99,9	10,2	0,891	39,9	12532
2500	2549	95,6	10,0	0,8916	37,6	9845
2000	2111	92,1	10,2	0,8838	36,1	7561
1500	1623	97,9	10,5	0,8881	38,453	6038
1000	1072	96,3	10,3	0,8874	37,8	3956

From Figure 8 can be seen, that the efficiency is strongly dependent on the transmitted load. For low transmitted torque the efficiency is very low, while in the proportion "Load : No Load" losses is low. It means the no load losses (i.e. the lubrication, sealing) play the majority. From the graphs can be clearly seen, that for precise measurement of influence of different design changes on efficiency of planetary sets, it will be necessary to change the lubrication system.

On Figure 9 we can observe slight decrease of efficiency with increase of speed of rotation. This influence can be again explained with splash lubrication.

To get an idea how big is the circulating torque/power with respect to the preload, following table brings the overview of measured and calculated data. The chosen example shows the data for maximal loading torque.

6. CONCLUSION

In the previous chapter the first measurement results were presented. When changing the splash lubrication with the pressure lubrication we can in the future obtain more precise data of the efficiency of the PGS. In the future is planned to measure:

- Influence of different bearing types of planets on efficiency, magnitude of axial force acting on planets.
- Influence of radial clearance of planets and number of planets on efficiency.
- Non-uniformity of load distribution on planets.
- Endurance test.

Although not all results are presented in the paper, the concept of the test stand is approved. The test stand is cheap, simple, easy to manipulate, with big potential for future measurements.

ACKNOWLEDGEMENT

This research has been realized using the support of The Ministry of Education, Youth and Sports program NPU I (LO), project # LO1311 Development of Vehicle Centre of Sustainable Mobility. The support is gratefully acknowledged.

LIST OF SYMBOLS

Unknowns

P	Power
M	Torque
n	Speed of rotation
i	Ratio
ς	Coefficient of losses
η	Efficiency

Subscripts

o	Circulation (power, torque)
a	Input
n	Output
m	Electric motor
1	Belonging to PGS 1
2	Belonging to PGS 2
r	Spider

REFERENCES

[1] Lechner G., Naunheimer H.: Automotive transmissions, Springer Verlag, 1999, ISBN 3-540-65903X

[2] Achtenova, G. and Milacek, O., "Innovative Configuration of the Closed-Loop Test Stand," SAE Technical Paper 2015-01-1092, 2015, doi:10.4271/2015-01-1092.

[3] Radev S., Einfluss von Flankenkorrekturen auf das Anregungsverhalten gerade – und Schrägverzahnter Stirnradpaarungen. Doktorarbeit TU München. 2007.

[4] http://www.strama-mps.de/produkte/pruefstaende/standards/fzg-zahnrad-verspannungspruefstand/

[5] Šalamoun Č.: The closed loop stand for planetary gearbox testing, In: Proc. of Mechanismen und Getriebe spanabhebender Werkzeugmaschinen, 1961 (in German)

[6] Rok J.: Design of planetary gear box for closed-loop test stand. Diploma work DP2012-MV05. CTU in Prague. 2012. (in Czech)

[7] Kazda L.: Proposal of the closed loop test stand. Diploma work. CTU in Prague. 2017. (in Czech)

[8] Moravec V., Havlík J., Folta Z., Achtenová G.: Analysis of Power Flow in Closed Loop Stands for Endurance tests of Gears and Transmissions, Journal MECCA 2/2004, ISSN 1214-0821

MASTER OF AUTOMOTIVE ENGINEERING

ENTRANCE LEVEL: Technical bachelor (mechanical, transport, or electro engineering)

CTU
Prague
Czech republic
(E)

ITB
Bandung
Indonesia
(E), (I)

ENSTA
Brest
France
(F)

TUCH
Chemnitz
Germany
(G)

3rd SEMESTER

Entrance exam IFP

ENSTA
- Design of Vehicles
- Modelisation and Computation

(F)

HAN
Vehicle Dynamics and Intelligent Transport Systems
(E)

CTU
Advanced Powertrains
(E)

TUCH
Alternative Powertrains
(G)

IFP
Paris
France
(F)+(E)

4th SEMESTER devoted to final thesis and 5 months internship in an industrial or academic environment anywhere in the world

MASTER DEGREE IN AUTOMOTIVE ENGINEERING
Master degree from 2 countries with respect to chosen specialisation in 3rd semester

(F) – in French, (E) – in English, (I) – in Indonesian, (G) – in German

CTU
Czech Technical University in Prague
Czech Republic
Gabriela Achtenová
gabriela.achtenova@fs.cvut.cz
Tel.: +420 224 352 499

ITB
Institut Teknologi Bandung
Indonesia
Andi Isra Mahyuddin
aim@ftmd.itb.ac.id

ENSTA
ENSTA Bretagne
France
Yann Marco
yann.marco@ensta-bretagne.fr
Tel.: +33 298 348 844

TUCH
Technische Universität Chemnitz
Germany
Diana Lohse
diana.lohse@mb.tu-chemnitz.de
Tel.: +49 371 531 337 94

HAN
Hogeschool van Arnhem en Nijmegen
The Netherlands
Kea Bouwman
kea.bouwman@han.nl
Tel.: + 31 26 384 93 14

DEADLINE FOR: NON EU STUDENTS 1ST MAY 2018, EU STUDENTS 30TH JUNE 2018
For application form, detailed programme, studying conditions, tuition fees and all other informations, please see: www.emae.eu

CZECH TECHNICAL UNIVERSITY IN PRAGUE

SCHOOL

ENSTA Bretagne

TECHNISCHE UNIVERSITÄT CHEMNITZ

Hogeschool van Arnhem en Nijmegen HAN University